

Design Considerations of Biaxially Tensile-Strained Germanium-on-Silicon Lasers

Xiyue Li^{a, b}, Zhiqiang Li^c, Simon Li^c, Lukas Chrostowski^d, and Guangrui (Maggie) Xia^b

^aSchool of Electronic and Information Engineering, South China University of Technology, Guangzhou, Guangdong
510641, China

^bDepartment of Materials Engineering, University of British Columbia, Vancouver, BC V6T 1Z4, Canada

^cCrosslight Software Inc., Vancouver, BC V5M 2A4, Canada

^dDepartment of Electrical and Computer Engineering, University of British Columbia, Vancouver, BC V6T 1Z4, Canada

Corresponding authors: Xiyue Li (email: lixiyue915@gmail.com), Guangrui(Maggie) Xia(email: gxia@mail.ubc.ca)

Abstract: Physical models of Ge energy band structure and material loss were implemented in LASTIPTM, a 2D simulation tool for edge emitting laser diodes. The model calculation is able to match experimental data available. Important design parameters of a Fabry-Perot Ge laser, such as the cavity length, thickness, width, polycrystalline Si cladding layer thickness were studied and optimized. The laser structure optimizations were shown to reduce the threshold current by 22-fold. The simulations also showed that improving the defect limited carrier lifetime is critical for achieving an efficient and low-threshold Ge laser. With the optimized structure design (300 μm for the cavity length, 0.4 μm for the cavity width, 0.3 μm for the cavity thickness, and 0.6 μm for the polycrystalline Si cladding layer thickness) and a defect limited carrier lifetime of 100 ns, a wall-plug efficiency of 14.6% at 1mW output is predicted, where J_{th} of 2.8 kA/cm^2 , I_{th} of 3.3 mA, $I_{1\text{mA}}$ of 9 mA, and η_d of 23.6% can also be achieved. These are tremendous improvements from the available experimental values at 280 kA/cm^2 , 756 mA, 837 mA and 1.9%, respectively.

Index Terms: Semiconductor lasers, semiconductor materials, optoelectronic materials, theory and design

1. Background and Introduction

Germanium is an indirect bandgap semiconductor, which is inferior in light emitting applications compared to direct bandgap semiconductors, such as GaAs and InP. However, it is the most Si-compatible semiconductor and plays an important role in Si photonics, such as detectors [1] and modulators [2]. In the past few decades, researchers all over the world have made extensive efforts in finding solutions to a Si-compatible lasing material system [3]-[17].

Breakthroughs were made by a group of MIT researchers, who demonstrated that Ge can become a gain medium sufficient for laser applications by adding tensile strain [18] and heavy n-type doping [19]. In 2010, an optically pumped Ge-on-Si laser was demonstrated using 0.2% biaxial tensile strain [20]. It operated at room temperature with a gain of 50 cm^{-1} at n-type doping of $1 \times 10^{19} \text{ cm}^{-3}$. The lasing was in a wavelength range of 1590 to 1610 nm. In 2012, an electrically pumped Ge-on-Si laser was demonstrated by the researchers from MIT and APIC Corporation, applying $4 \times 10^{19} \text{ cm}^{-3}$ n-type doping and 0.25% biaxial tensile strain [21]. The lasing wavelengths were between 1520 and 1700 nm with a variation consistent with different clamping condition. In 2015, lasing was observed from an electrically pumped $3 \times 10^{19} \text{ cm}^{-3}$ n-type doped Ge Fabry-Perot resonator on Si by R. Koerner et al.[22], confirming the principal validity of early work of Prof. Kimerling's group at MIT in Refs. [20], [21].

Introducing tensile strain to Ge is crucial to change Ge from an indirect bandgap material into a direct bandgap material [18], [21]. Both biaxial and uniaxial tensile strain can make this transition. Many efforts have been made to increase tensile strains in Ge. The standard one relied on the thermal expansion coefficient mismatch during the growth and cooling process of Ge on Si layer [18]. It can lead to approximately 0.25% biaxial tensile strain in Ge layers. G. Capellini *et al.* used silicon nitride layer to stress Ge up to about 0.9% biaxial tensile strain, and the fabrication process was COMS-compatible [23]. D. S. Sukhdeo *et al.* from Stanford used a stress concentration method in Ge-on-insulator (GOI) substrates, and obtained 5.7% uniaxial tensile stress in Ge bridges. Their work also showed that at 4.6% uniaxial tensile strain Ge changes to a direct bandgap material [24]. On the doping technologies, multi-layered delta-doped layers were used to create source phosphorous (P) concentration above $1 \times 10^{20} \text{cm}^{-3}$ and achieve active carrier concentration above $4 \times 10^{19} \text{cm}^{-3}$ [25][26].

On the theoretical modeling side, the gain calculation model and a threshold current density model were described by Cai and Han *et al.* [27]. With the bandgap narrowing effect and the energy separation effect for heavily n-type doped Ge, good agreements with the experiment data can be obtained. W. W. Chow also described a gain theory for a bulk Ge active medium taking the many-body Coulomb effect into account [28]. B. Dutt *et al.* studied the Ge doping and strain impacts on slope efficiencies with some simplified assumptions without taking the cavity dimensions into account [29].

As an early demonstration, the laser in Ref. [21] had an extremely high threshold current, which limited its operation efficiency. To shed some light on the laser design and performance improvements, two-dimensional (2D) device simulations are in great need. Little work is available on 2D laser device simulations, and key device performance parameters such as threshold current and wall-plug efficiencies have not been well-studied, which will be addressed in this work.

In this work, models of Ge energy band structure (with biaxial strain and doping) and material loss (including the bandgap narrowing effect and the energy separation effect) were implemented in LASTIPTM, a 2D simulation tool for edge emitting laser diodes. With this capability, simulations of a Ge Fabry-Perot laser under biaxial tensile strain were made to investigate the important design parameters and to optimize the Ge laser performance.

2. Optical gain model and parameters used

The biaxial tensile strain impact on Ge energy bandgap structure has been well studied, and a biaxial tensile strain can be considered as a combination of a hydrostatic strain component plus a uniaxial strain component [30], [31]. The strain related Ge energy band models in Refs. [30], [31] was implemented in LASTIPTM. Doping induced bandgap narrowing effect (BGN) is non-negligible [32]. The direct bandgap narrowing effect (ΔE_g^Γ) model from Ref. [32] was implemented in LASTIPTM, while the indirect bandgap narrowing effect ΔE_g^L was assumed the same as ΔE_g^Γ [27]. The effective mass values of electrons and holes in Ge we used are from Ref. [18].

Gain calculations were made for Ge with 0.25% biaxial tensile strain and $4 \times 10^{19} \text{cm}^{-3}$ n-type doping at different carrier injection levels, as shown in Fig. 1. The calculations are consistent with literature work in Ref. [27]. The kinks at about $\lambda = 1720 \text{ nm}$ show that the quasi-Fermi level F_v has already entered the HH band inducing fast rise in gain coefficient due to significantly increased density of states.

In the low strain region ($\epsilon_{xx} < 0.6\%$), the gain spectra maximum is associated with the direct band to band transition involving heavy hole band (HH band) that indeed hosts the majority of valence carrier [33], which means population inversion into HH band is required to overcome free carrier losses.

Direct transitions between Γ_c and light hole (LH) states will occur for larger values of biaxial strain [29]. These favor that the Ge light emission under 0.25% tensile strain is operating in TE mode, which is relevant to the HH transition [33]. Additionally, for the Ge laser simulated in Ref. [21], the losses for TM modes are very large due to the metal contact, and only TE modes have low enough losses for light emission [26].

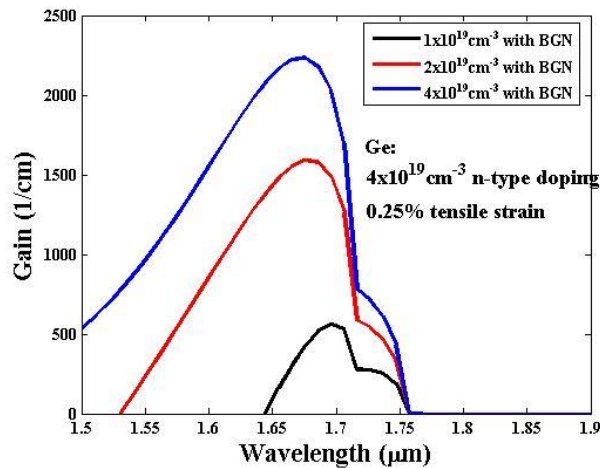


Fig.1. Gain spectra from direct transition in 0.25% tensile strained n^+ Ge with $4 \times 10^{19} \text{ cm}^{-3}$ doping at different carrier injection level.

3. Optimizations of an electrically pumped Fabry-Perot Germanium laser

The experimental work in Ref. [21] showed a lasing range from 1520 nm to 1700 nm, a threshold current density (J_{th}) of 280 kA/cm^2 , and a differential quantum efficiency of 1.9%. The reason for this high J_{th} is due to the non-optimized cavity dimensions, the fabrication imperfections including high series resistance from the top poly-Si contact, large free carrier absorption, metals contacts as well as the high diode leakage current [27]. Moreover, only 1 mW of output was observed despite the high current density of 310 kA/cm^2 was driven into the 270 μm long Ge cavity. The device cannot be practical without both drastic reduction in the threshold current and a vastly improved efficiency. Therefore, investigating methods to optimize and improve the Ge laser performance is the main target of this work. Although Ge lasers can also be used in long distance optical communications, the target application and thus the performance optimization of this work are for the on-chip optical interconnects. After the Ge cavity and cladding thickness optimization to reduce the threshold current (I_{th}), the effect of defect limited carrier time is also taken into account. No thermal effects are included in this work.

3.1. Laser structure, parameters to optimize and optimization criteria

In this work, we investigated the design optimization of an electrically pumped Ge-on-Si double heterojunction Fabry-Perot laser, and the cross section of this laser is shown in Fig. 2. The laser structure, the top metal contact, doping and strain are the same as the experiment reported in Ref. [21]. The bottom metal contact is not shown as it is sufficiently far away. Only 2 μm Si substrate is included in the simulations, which is set to be $5 \times 10^{19} \text{ cm}^{-3}$ n-type doped [26]. A virtual contact was defined underneath the bottom of the 2 μm Si substrate for biasing purpose and has no interactions with photons or the light intensity distribution.

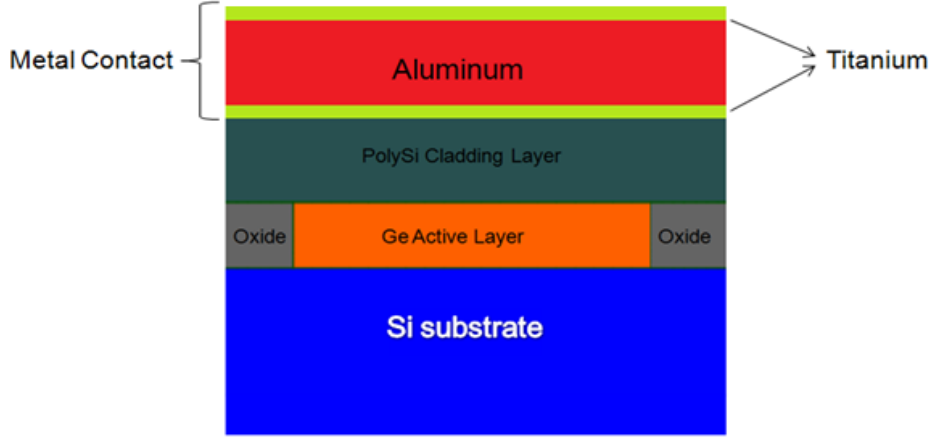


Fig. 2. Cross section of the Ge-on-Si heterojunction laser structure simulated.

The parameters to optimize are the Ge cavity length, thickness, width, and the poly-Si cladding thickness. In our optimization, five figures of merits are discussed. First, the threshold current density J_{th} is used so that our simulation can be compared with available experimental data or simulations. For the Ge thickness and poly-Si thickness dependence study, as no cross-section area change is involved, J_{th} and the threshold current I_{th} share the same trend. Then, in the light power-current (L-I) plots, I_{th} and the current at 1 mW optical output power (I_{1mW}) are quoted. The choice of 1 mW is just for the convenience of discussion. The differential quantum efficiency η_d and the wall-plug efficiency η_{wp} are calculated to benchmark the Ge laser efficiency in converting electrical power to light power. Among all the figures of merits, the most important optimization criterion is the threshold current I_{th} .

3.2. Material parameters used

Many performance parameters depend on the lasing material growth and processing techniques, which we assumed to be the same as the material in Ref. [21][27]. The reflectivity values of two facet are $R_1 = 23\%$ and $R_2 = 38\%$, and the corresponding mirror loss α_m is 45 cm^{-1} , all taken from Ref. [27]. The index of refraction of Ge is set to be 4.2 [34].

In this work, we assume that the internal loss and the mirror loss are the main sources of absorption, and the internal loss is dominated by the free carrier absorption [35]. In LASTIPTM, for a narrow wavelength range, the free carrier absorption is described by

$$\alpha_i = AN + BP, \quad (1)$$

where A and B are constants, N and P are electron and hole density in units of cm^{-3} . In lasing around 1700 nm, by using the free carrier absorption results with first principle calculation in n-type doped Ge [27] [36] and fitting the experimental data in p-type doped Ge [37] at room temperature, we obtained

$$\alpha_i = 5.0 \times 10^{-18} N + 1.03 \times 10^{-18} P, \quad (2)$$

where α_i is in units of cm^{-1} . The free carrier absorption relations for the doped Si substrate and poly-Si cladding layer are from well-quoted work in Refs. [38] and [39], where λ is the wavelength in units of micrometers

For Si:

$$\alpha_i(\lambda) = 1.8 \times 10^{-18} N \lambda^2 + 2.7 \times 10^{-18} P \lambda^2 \quad (3)$$

For poly-Si (at $\lambda=1.55 \text{ }\mu\text{m}$):

$$\alpha_i(\lambda) = 1.079 \times 10^{-17} N + 7.47 \times 10^{-18} P \quad (4)$$

3.3. Fitting the experimental data and model calibration

For on-chip optical interconnect applications, it is highly desirable to have I_{th} as low as possible. The data available in experimental work Ref. [21] have a J_{th} of 280 kA/cm^2 , which corresponds to $I_{th} = 756 \text{ mA}$, and a differential quantum efficiency of 1.9%. We need to first calibrate our models with the experimental data. For that purpose, we set the structure, doping and stress parameters same as those in Ref. [21], which is under 0.25% biaxial tensile strain and $4 \times 10^{19} \text{ cm}^{-3}$ n-type doping, $1 \mu\text{m}$ Ge width, $270 \mu\text{m}$ length and 180 nm poly-Si cladding layer thickness. The Ge active layer thickness was set to be 200 nm , which is the average value of the $100\text{--}300 \text{ nm}$ thickness in the experiment due to the non-uniform interface [21][26]. The defect limited carrier lifetime in epitaxial grown Ge film is conservatively assumed to be 1 ns for this thickness as measured in recent Refs. [40], [41]. However, those measurements were not performed on junction structures, where the field near the junctions could place the minority carriers away from the highly defected Ge/Si interfaces. The two fitting parameters we used to fit the experimental optical power vs. the injected current density characteristics are the Auger coefficients C_{ppn} and C_{nnp} . The best fitting Auger coefficients are $C_{nnp} = 3.0 \times 10^{-32} \text{ cm}^6/\text{s}$ and $C_{ppn} = 7.0 \times 10^{-32} \text{ cm}^6/\text{s}$ [18].

Using these parameters, our models produce a J_{th} of 290 kA/cm^2 and a I_{th} of 790 mA at 15°C with the TE mode at $\lambda = 1680 \text{ nm}$, which is relevant to the gain peak location in Fig. 1, very close to the experimental value of 280 kA/cm^2 [21]. As seen in Fig.3, the models can match the experimental laser output characteristics quite well. After the calibration of our models, we started optimizing the laser structure. The Ge length dependence was first studied.

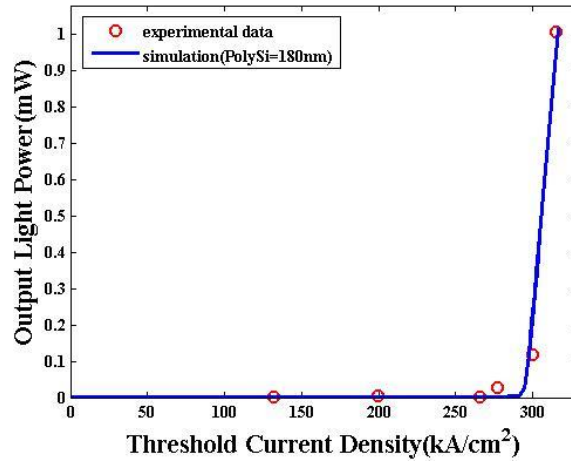


Fig.3. Comparisons between the results using our models and the experimental data from Ref. [21] at 15°C (Ge length: $270 \mu\text{m}$, Ge thickness: 200 nm , Ge width: $1 \mu\text{m}$, poly-Si thickness: 180 nm).

3.4. Ge cavity length dependence

To optimize the Ge cavity length, the optical power vs. the injected current (L-I) characteristics were simulated for a range of Ge cavity length from $270 \mu\text{m}$ to 1 mm with other parameters unchanged. Theoretically, the longer cavity can both generate more power and reduce mirror loss. The cavity length of common compound semiconductor lasers can reach as long as 1 mm . However, larger threshold current is not desired for on-chip interconnects applications. Therefore, there still is an optimal cavity length for the lowest I_{th} . In our simulations, I_{th} and I_{1mW} can be obtained by the L-I plots.

Just as it is desirable to have as low I_{th} as possible, it is also desirable to have an efficient laser. From these two current values I_{th} and I_{1mW} , we can deduct the differential quantum efficiency η_d [42],

$$\eta_d = \frac{\Delta P}{\Delta I} \bigg/ \frac{hc}{q\lambda} \quad (5)$$

$$\frac{\Delta P}{\Delta I} \approx \frac{1mW}{I_{1mW} - I_{th}}, \quad (6)$$

where c is the speed of light and h is the Planck's constant.

Starting from this part, as there are no experimental J_{th} data to compare to, I_{th} is used as the optimization criteria. η_d can be calculated from I_{th} and I_{1mW} using Eqs. (5) and (6). The I_{th} behavior can be expressed with the following equations [42]:

$$I_{th} = \frac{\frac{n}{c} \frac{1}{\Gamma \tau_p G} + n_{tr}}{\tau_s \eta_i} qWLd = J_{th}WL \quad (7)$$

$$\frac{1}{\tau_p} \cdot \frac{n}{c} = \alpha_i + \alpha_m = \alpha_i + \frac{1}{2L} \ln\left(\frac{1}{R_1 R_2}\right), \quad (8)$$

where n , G , τ_p , τ_s , η_i , n_{tr} , W , L and d are the group index of refraction, the proportionality factor between the gain and the carrier density, the photon life-time, the electron-hole recombination lifetime, the internal quantum efficiency, the carrier density at transparency, the cavity width, the cavity length and the cavity thickness.

Fig. 4 shows J_{th} , I_{th} and I_{1mW} at room temperature with different cavity lengths. In Fig. 4(b), we can see that there is a minimum I_{th} at cavity length of 300 μm . According to Eq. (7) and (8), when L is too small, more gain and mirror loss are needed, where the differential gain is smaller, resulting in a larger I_{th} . When L is too long, more current is needed to bring a large volume to transparency, which results in a monotonically increase in I_{th} , even in the region longer than 1 mm. The cavity length optimization slightly reduces the threshold current from 790 mA to 780 mA.

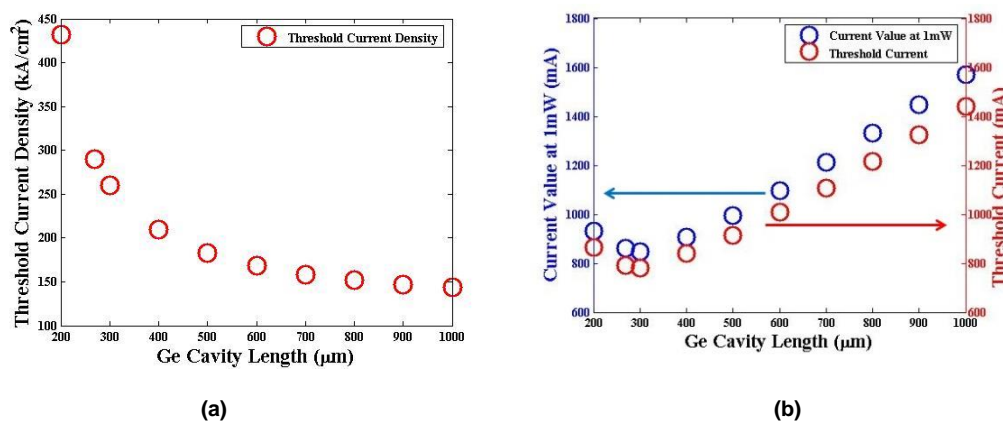


Fig.4. (a) J_{th} dependence of the Ge cavity length L ; (b) I_{th} and I_{1mW} dependence of cavity length L (Ge thickness: 200 nm, Ge width: 1 μm , poly-Si thickness: 180 nm).

3.5. Ge cavity thickness dependence

In this section we investigated the Ge cavity thickness impact on the laser performance with the optimized cavity length at 300 μm . J_{th} can be expressed as [43]

$$\eta_i \frac{J_{th}}{qd} = (An_{th} + Bn_{th}^2 + Cn_{th}^3) \quad (9)$$

$$n_{th} = n_r + \frac{\alpha_i + \alpha_m}{\Gamma(d)G}, \quad (10)$$

where d is the Ge cavity thickness, Γ is the optical confinement factor, n_{th} is the carrier density at threshold condition, A and C describe non-radiative recombination due to traps and surface and Auger process, respectively, B is radiative recombination coefficient, G' is G/Γ , which is a material parameter. In Eq. (10), we can see that n_{th} has thickness dependence because of Γ . In this section, because the cross-section area is constant, J_{th} and I_{th} share the same trend.

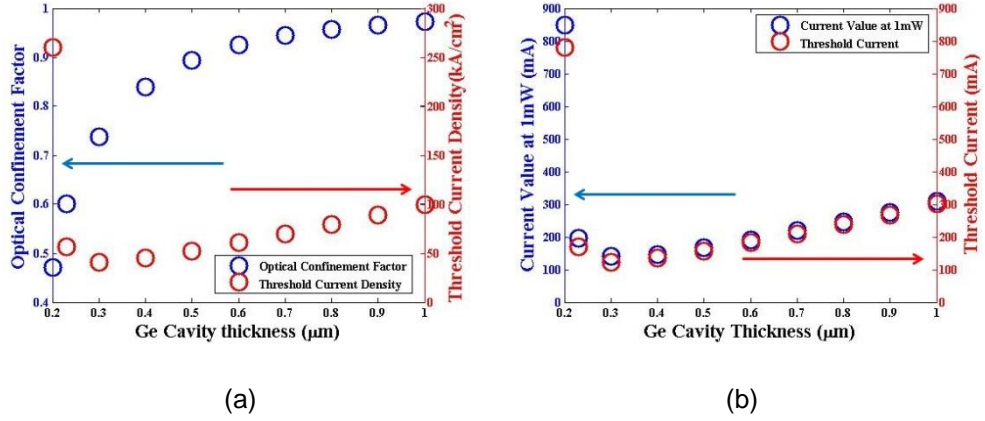


Fig. 5. (a) Optical confinement factor and Threshold current density dependence of the Ge cavity thickness in the range of 0.2~1 μm ; (b) Threshold current and Current value at output light power of 1mW between the Ge cavity thickness varied from 0.2~1 μm (Ge length: 300 μm , Ge width: 1 μm , poly-Si thickness: 180 nm).

Fig. 5 shows the calculated I_{th} as a function of Ge cavity thickness d at Ge width of 0.2~1 μm . We can see that the lowest I_{th} is obtained at Ge thickness of around 0.3 μm . When the Ge thickness d is too thin, an increasing fraction of the optical intensity is outside the active region due to the smaller optical confinement factor Γ , we can see that in thinner thickness, the J_{th} and I_{th} are significantly affected by the optical confinement factor Γ . On the thicker end, Γ is approaching 1, and I_{th} is linear with d . The laser will also be more efficient with a bigger thickness due to the relevant bigger active lasing region. The optimum I_{th} is around $d = 0.3 \mu\text{m}$, where the emission wavelength will also red shift with the increasing thickness [21] to $\lambda = 1700 \text{ nm}$. The cavity thickness optimization reduces the threshold current from 780 mA to 123 mA.

3.6. Ge cavity width dependence

With the optimized Ge cavity length of 300 μm and thickness of 0.3 μm , next, we investigated the cavity width's influence on the Ge laser. Fig. 6(a) shows J_{th} vs. different cavity width W with the optimized Ge length, thickness and the fixed poly-Si thickness of 180 nm, respectively. According to Eq. (7), with the decreasing cavity width, J_{th} became higher due to the decrease of the optical confinement factor, which can be also seen in Fig. 6(a).

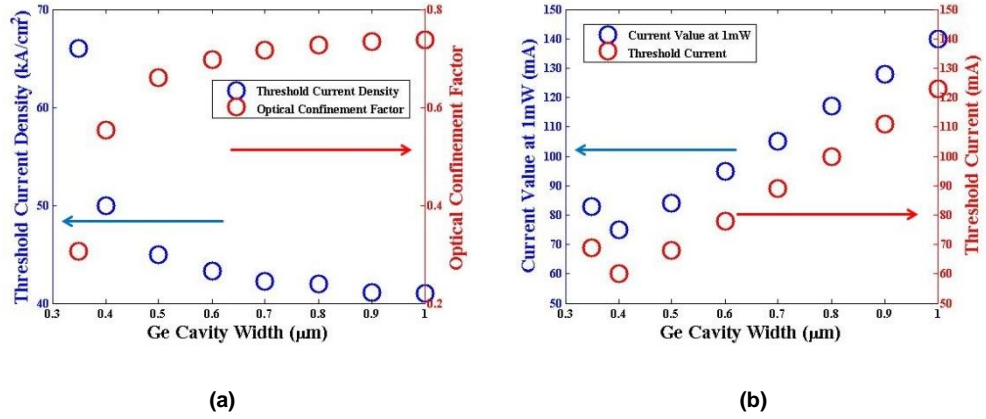
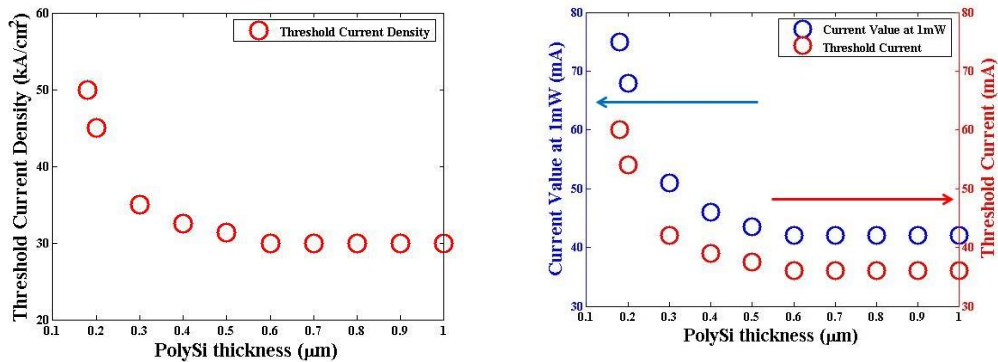


Fig.6. (a) Optical confinement factor and Threshold current density dependence of the Ge cavity width in the range of 0.3~1 μm ; (b) Threshold current and Current value at output light power of 1mW between the Ge cavity width varied from 0.3~1 μm (Ge length: 300 μm , Ge thickness: 0.3 μm , poly-Si thickness: 180 nm).

When considering the I_{th} , it has a different W dependence. A wider laser requires more injection current to reach the onset of the lasing action. We can see that in Fig. 6(b) that between 0.3 μm to 1 μm , the lowest threshold current value is at Ge cavity width around 0.4 μm . When cavity width is below 0.4 μm , a decreasing proportion of active region for light emission in the device will cause a higher I_{th} . In Fig. 6(b), $I_{1\text{mW}}$ is also shown. The similar trend between I_{th} and $I_{1\text{mW}}$ for $W > 0.4 \mu\text{m}$ is expected as Γ and thus η_d is not sensitive to Ge width in this range, due to the large difference between the refractive index in Ge and SiO_2 . The cavity width optimization reduces the threshold current from 123mA to 60 mA.

3.7. Poly-Si cladding thickness dependence

Now that we have determined the Ge cavity size (thickness, width and length are 0.3 μm , 0.4 μm and 300 μm , respectively), we can optimize the thickness of the poly-Si cladding layer. The high J_{th} 280 kA/cm^2 in the experimental data is partially due to the lossy metal contact, where the poly-Si thickness was 180 nm. If the metal contact is moved further away from the Ge cavity, the losses would decrease monotonically. The simulation results are shown in Fig. 7. We chose the optimal thickness of the poly-Si layer to be 0.6 μm , above which the extra decrease in I_{th} is negligible. It can also be seen that the difference in I_{th} and $I_{1\text{mW}}$ shrinks in each optimization step, showing an increase in η_d . The Poly-Si cladding thickness optimization reduces the threshold current from 60 mA to 36 mA. Compared to the original 790 mA, it is a 22-fold reduction after all the structure optimizations.



(a)

(b)

Fig.7. (a) J_{th} dependence of the poly-Si thickness in the range of 0.18 to 1 μm ; (b) I_{th} and I_{1mA} between the poly-Si thickness in the range of 0.18 to 1 μm (Ge length: 300 μm , Ge thickness: 0.3 μm , Ge width: 0.4 μm).

3.8. Defect limited carrier lifetime dependence

With the optimized Ge cavity size (thickness 0.3 μm , width 0.4 μm , length 300 μm) and the poly-Si cladding layer thickness (0.6 μm), as shown in Fig.8 (a), our models predict that J_{th} of 30 kA/cm^2 , I_{th} of 36 mA, I_{1mA} of 42 mA and V_{1mA} of 0.84V. The wall-plug efficiency η_{wp} of 2.8% can be achieved with 1 ns defect limited carrier lifetime. The result is far away from the common commercial compound semiconductor lasers which have wall-plug efficiencies in the range of 20~30%. As previously discussed in 3.3, 1 ns lifetime is a conservative estimation. For the laser in Ref. [21], carriers were concentrated at the p-n junction, which was designed to be away from the highly defected Ge/Si interfaces. Technically, it is also feasible to growth high quality thick Ge layers, bond them to a handle wafer, etch back and polish away the highly defected Ge buffer layers, which generates Ge layers with much better quality and longer carrier lifetime. To investigate the impact of the carrier lifetime, we performed simulations with various carrier lifetimes up to that of bulk Ge (100 ns) with all other conditions unchanged [44]. With a 100 ns lifetime, the performance of the Ge laser can be greatly improved, predicting a J_{th} of 2.8 kA/cm^2 , I_{th} of 3.3 mA, I_{1mA} of 9 mA, V_{1mA} of 0.76V and η_{wp} of 14.6% (Fig. 8). This makes the Ge laser performance much closer to that of common III-V semiconductor lasers. The threshold current I_{th} and wall-plug efficiency η_{wp} of the Ge laser for various defect limited carrier lifetime can be seen in Fig. 9 showing the essential role of minority carrier lifetime on the threshold current reduction and the efficiency enhancement. This is consistent with the recent work by D. S. Sukhdeo et al. [44].

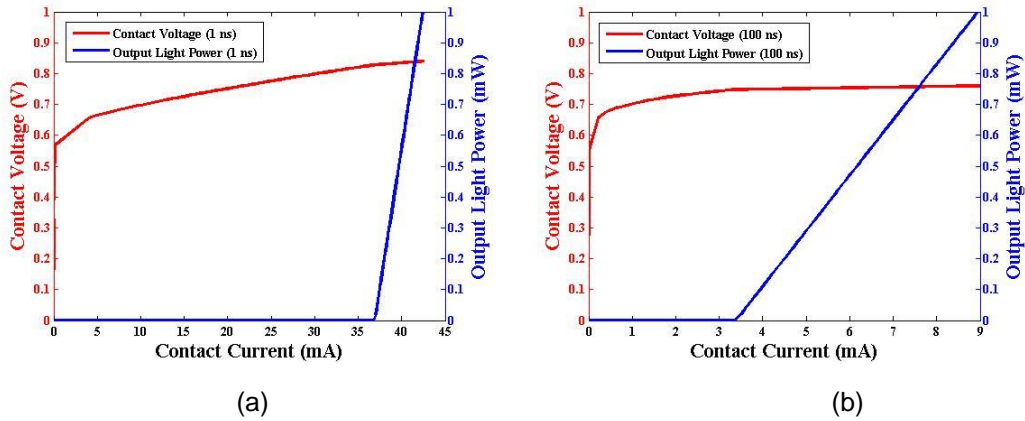


Fig.8. Optimized L-I and Contact Voltage-Contact Current characteristics with defect limited carrier lifetime 1 ns (a) and 100 ns (b) (Ge: thickness 0.3 μm , width 0.4 μm , length 300 μm , poly-Si: cladding thickness 0.6 μm)

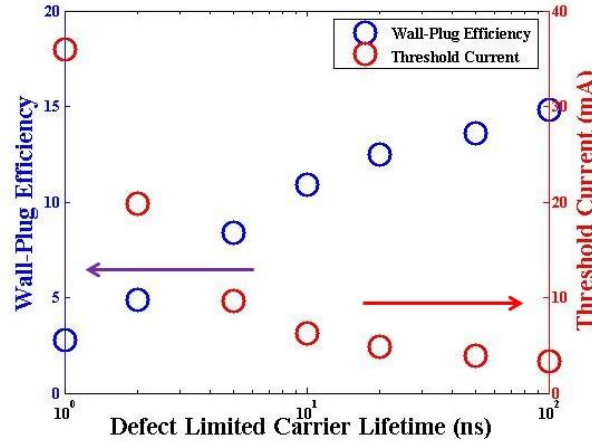


Fig.9. wall-plug efficiency of the Ge laser for various defect limited carrier lifetime

4. Conclusions

Physical models of Ge energy band structure and material loss were implemented in LASTIPTM, a 2D simulation tool for edge emitting laser diodes. The model calculation is able to match experimental data available. Important design parameters of a Fabry-Perot Ge laser, such as the cavity length, thickness, width, polycrystalline Si cladding layer thickness were studied and optimized. The laser structure optimizations were shown to reduce the threshold current by 22-fold. The simulations also showed that improving the defect limited carrier lifetime is critical for achieving an efficient and low-threshold Ge laser. With the optimized structure design (300 μm for the cavity length, 0.4 μm for the cavity width, 0.3 μm for the cavity thickness, and 0.6 μm for the polycrystalline Si cladding layer thickness) and a defect limited carrier lifetime of 100 ns, a wall-plug efficiency of 14.6% at 1mW output is predicted, where J_{th} of 2.8 kA/cm^2 , I_{th} of 3.3 mA, $I_{1\text{mA}}$ of 9 mA, and η_d of 23.6% can also be achieved. These are tremendous improvements from the available experimental values at 280 kA/cm^2 , 756 mA, 837 mA and 1.9%, respectively.

Considering that common commercial compound semiconductor lasers have wall-plug efficiencies in the range of 20-30%, that of the optimized Ge laser is about half of that. Strain, doping, quantum-well structure and material quality optimization, although outside the scope of this work, are all very important to improve the Ge laser performance. With future efforts in all other design and processing aspects, we are optimistic to expect Ge lasers with much better performance realized in the near future.

Acknowledgments

This work was supported by the Oversea Study Program of Guangzhou Elite Project. The authors would like to thank Mr. Michel Lestrade from Crosslight software for his assistance in LASTIPTM usage, Mr. Yiheng Lin from the Department of Materials Engineering at the University of British Columbia and Prof. Jifeng Liu from Thayer School of Engineering at Dartmouth College for helpful discussions.

References

- [1] A. K. Okyay, A. M. Nayfeh, T. Yonehara, A. Marshall, P. C. McIntyre, and K. C. Saraswat, "Ge on Si by Novel Heteroepitaxy for High Efficiency Near Infrared Photodetection," presented at the Proc. CLEO, Long Beach, CA, 2006, CTuU5.

- [2] J.E. Roth, O. Fidaner, R.K. Schaevitz, Yu-Hsuan Kuo, T.I. Kamins, J.S. Harris, and D.A. B. Miller, "Optical modulator on silicon employing germanium quantum wells," *Opt. Express*, vol.15, no.9, pp.5851-5859, Apr. 2007.
- [3] A.G. Cullis, L.T. Canham, "Visible light emission due to quantum size effects in highly porous crystalline silicon," *Nature*, vol.353, no. 6342, pp. 335 – 338, Sep. 1991.
- [4] A.G. Cullis, L.T. Canham and P.D.J. Calcott, "The structural and luminescence properties of porous silicon," *J. Appl. Phys.*, vol. 82, no.3, pp. 909–965, 1997.
- [5] S.Schuppler, S.L. Friedman, M.A. Marcus, D.L. Adler, Y.-H. Xie, F.M. Ross, Y.J. Chabal, T.D. Harris, L.E. Brus, W.L. Brown, E.E. Chaban, P.F. Szajowski, S.B. Christman, and P.H. Citrin, "Size, shape, and composition of luminescent species in oxidized Si nanocrystals and H-passivated porous Si," *Phys. Rev. B*, vol. 52, no.7, pp. 4910–4925, Aug. 1995.
- [6] Y. Kanemitsu, "Light emission from porous silicon and related materials," *Phys. Rep.*, vol.263, no.1, pp.1–91, 1995.
- [7] Z.H. Lu, D.J. Lockwood and J.-M.Baribeau, "Quantum confinement and light emission in SiO₂/Si superlattices," *Nature*, vol. 378, no.6554, pp. 258–260, 1995.
- [8] K.D. Hirschman, L. Tsybeskov, S.P. Duttagupta and P.M. Fauchet, "Silicon-based visible lightemitting devices integrated into microelectronic circuits," *Nature*, vol. 384, no.6607, pp. 338–341, 1996.
- [9] L. Tsybeskov, K.D. Hirschman, S.P. Duttagupta, M. Zacharias, P.M. Fauchet, J.P. McCaffrey, D.J. Lockwood, "Nanocrystalline-silicon superlattices produced by controlled recrystallization," *Appl. Phys. Lett.*, vol.72, no.1, pp. 43–45 Jan. 1998.
- [10] G.F. Grom, D.J. Lockwood, J.P. McCaffrey, H.J. Labbe, P.M. Fauchet, B. White, J. Diener, D. Kovalev, F. Koch and L. Tsybeskov, "Ordering and self-organization in nanocrystalline silicon," *Nature*, vol. 407, no.6802, pp. 358–361, Sep. 2000.
- [11] A.L. Efros, D.J. Lockwood, L. Tsybeskov, *Semiconductor Nanocrystals: From Basic Principles to Applications*, Kluwer Academics/Plenum Publishers Press, 2003.
- [12] L. Pavesi, L. Dal Negro, C. Mazzoleni, G. Franzo and F. Priolo, "Optical gain in silicon nanocrystals," *Nature*, vol.408, no.6811, pp.440–444, Nov.2000.
- [13] S. Coffa, G. Franzò, F. Priolo, "High efficiency and fast modulation of Er-doped light emitting Si diodes," *Appl. Phys. Lett.*, vol. 69, no.14, pp. 2077–2079, Sep.1996.
- [14] S. Fukatsu, N. Usami, Y. Shiraki, A. Nishida and K. Nakagawa, "High-temperature operation of strained Si_{0.65}Ge_{0.35}/Si(111) p-type multiple-quantum-well light-emitting diode grown by solid source Si molecular-beam epitaxy," *Appl. Phys. Lett.*, vol.63, no.7, pp. 967–969, 1993.
- [15] R. Apetz, L. Vescan, A. Hartmann, C. Dieker and H. Luth, "Photoluminescence and electroluminescence of SiGe dots fabricated by island growth," *Appl. Phys. Lett.*, vol. 66, no.4, pp. 445–447, Jan.1995.
- [16] D.C. Houghton, J.-P. Noël, and N.L. Rowell, "Electroluminescence and photoluminescence from Si_{1-x}Ge_x alloys grown on (100) silicon by molecular beam epitaxy," *Mater. Sci. Eng.* vol. 9, no.1–3, pp. 237–244, July.1991.
- [17] D. Leong, M. Harry, K.J. Reeson, K.P. Homewood, "A silicon/iron-disilicide light-emitting diode operating at a wavelength of 1.5 μm ," *Nature*, vol. 387, no. 6634, pp. 686–688, 1997.
- [18] J. Liu, X. Sun, D. Pan, X. Wang, L. C. Kimerling, T. L. Koch, and J. Michel, "Tensile-strained, n-type Ge as a gain medium for monolithic laser integration on Si," *Opt. Express*, vol. 15, no. 18, pp.11272–11277, Aug.2007.
- [19] Y. Cai and R. Camacho-Aguilera, "High n-type doped germanium for electrically pumped Ge laser," in Advanced Photonics Congress, OSA Technical Digest (online) (Optical Society of America, 2012), paper IM3A.5.
- [20] J. Liu, X. Sun, R. Camacho-Aguilera, L. C. Kimerling, and J. Michel, "Ge-on-Si laser operating at room temperature," *Opt. Lett.*, vol. 35, no.5, pp. 679–681, Mar.2010.
- [21] J. Michel, R. E. Camacho-Aguilera, Y. Cai, N. Patel, J. T. Bessette, M. Romagnoli, R. Dutt, and L. Kimerling, : An electrically pumped Ge-on-Si laser, in Optical Fiber Communication Conference, OSA Technical Digest (Optical Society of America, 2012), paper PDP5A.6.
- [22] R. Koerner, M. Oehme, M. Gollhofer, M. Schmid, K. Kostecky, S. Bechler, D. Widmann, E. Kasper, J. Schulze, "Electrically

- pumped lasing from Ge Fabry-Perot resonators on Si", *Opt. Express*, vol.23, no.11, pp.14815-14822, Jun 2015.
- [23] G.Capellini, C.Reich, S.Guha, Y.Yamamoto, M.Lisker, M.Virgilio, A.Ghrib, M.El Kurdi, P.Boucaud and B.Tillack, "Tensile Ge microstructures for lasing fabricated by means of a silicon complementary metal-oxide-semiconductor process", *Opt. Express*, vol.22, no.1, pp.399-410, Jan 2014.
- [24] D.S. Sukhdeo, D. Nam, J.-H. Kang, M.L. Brongersma, and K.C. Saraswat, "Direct bandgap germanium-on-silicon inferred from 5.7% $\langle 100 \rangle$ uniaxial tensile strain [Invited]", *Photonics Research*, vol.2, no.3, pp. A8-A13, Jun.2014.
- [25] R.E. Camacho-Aguilera, Y.Cai, J.T. Bessette, L. C. Kimerling, and J. Michel, "High active carrier concentration in n-type, thin film Ge using delta-doping," *Optical Materials Express*, vol.2, no.11, pp.1462-1469, Nov.2012.
- [26] R.E. Camacho-Aguilera, "Ge-on-Si LASER for Silicon Photonics", Ph. D dissertation, Department of Materials Science and Engineering, Massachusetts Institute of Technology, 2013.
- [27] Y. Cai, Z. Han, X. Wang, R.E. Camacho-Aguilera, L.C. Kimerling, J. Michel, and J. Liu, "Analysis of Threshold Current Behavior for Bulk and Quantum Well Germanium Laser Structures," *IEEE Journal of Selected Topics in Quantum Electronic*, vol. 19, no.4, p.1901009, Jul.2013.
- [28] W.W.Chow, "Model for direct-transition gain in a Ge-on-Si laser," *Appl. Phys. Lett.*, vol.100, no.19, p.191113, May.2012.
- [29] B. Dutt, D.Sukhdeo, D. Nam, B.M. Vulovic, Z. Yuan and K.C. Saraswat, "Roadmap to an Efficient Germanium-on-Silicon Laser: Strain vs. n-Type Doping," *IEEE Photonics Journal*, vol. 4, no.5, pp. 2002-2009, Oct.2012.
- [30] D.J Paul, "Si/SiGe heterostructures: from materials and physics to devices and circuits," *Semicond. Sci. Technol.*, vol.19, no.10, pp. R75-R108, Oct.2004.
- [31] Karl Brunner, "Si/Ge nanostructures," *Rep. Prog. Phys.*, vol.65, no.1, pp. 27-72, Jan.2002.
- [32] R.Camacho-Aguilera, Z. Han, Y. Cai, L.C. Kimerling and J. Michel, "Direct band gap narrowing in highly doped Ge," *Appl. Phys. Lett.*, vol.102, no.15, p.152106, Apr.2013.
- [33] M.Virgilio, C.L.Manganelli, G.Grosso, G.Pizzi, G.Capellini, "Radiative recombination and optical gain spectra in biaxially strained n-type germanium", *Physical Review B*, vol.87,no.23, p.235313, Jun 2013.
- [34] Y.Cai, "Materials Science and Design for Germanium Monolithic Light Source on Silicon", Ph. D dissertation, Department of Materials Science and Engineering, Massachusetts Institute of Technology, 2014.
- [35] R. E. Camacho-Aguilera, "Monolithically-integrated Ge CMOS laser", SPIC Proceedings, vol.9010, Feb, 2014.
- [36] J.Liu, "Monolithically Integrated Ge-on-Si Active Photonics", *Photonics*, vol.1, no.3, pp.162-197, July 2014.
- [37] R.Newman and W.W.Tyler, "Effect of impurities on free-hole infrared absorption in p-type germanium", *Physical Review*, vol.105,no.3, pp. 885-886, Feb.1957.
- [38] D. K. Schroder, R.N. Thomas, J.C. Swartz, "Free Carrier Absorption in Silicon," *IEEE Journal of Solid-State Circuits*, vol.13, no.1, pp.180-187, 1978.
- [39] Oshoriamhe Ogah, "Free-carrier effects in polycrystalline silicon-on-insulator photonic devices", M.S. thesis, Microelectronic Engineering, Rochester Institute of Technology, 2010.
- [40] R. Geiger, J. Frigerio, M. J. Süess, D. Chrastina, G. Isella, R. Spolenak, J. Faist, and H. Sigg, "Excess carrier lifetimes in Ge layers on Si," *Appl. Phys. Lett.*, vol. 104, no. 6, p. 062106, Feb. 2014.
- [41] D. Nam, J.-H. Kang, M. L. Brongersma, and K. C. Saraswat, "Observation of improved minority carrier lifetimes in high-quality Ge-on-insulator using time-resolved photoluminescence," *Opt. Lett.*, vol. 39, no. 21, p. 6205, Oct. 2014.
- [42] A. Yarif and P. Yeh, *Photonics: Optical Electronics in Modern Communications*, Oxford, U.K.; Oxford University Press, 6th Revised edition, 2006.
- [43] S.L. Chuang, *Physics of Photonic Devices*, John Wiley & Sons Press, 2nd Revised edition, 2009).
- [44] D.S. Sukhdeo, K.C. Saraswat, B. Dutt and D. Nam, "Impact of Minority Carrier Lifetime on the Performance of Strained Ge Light Sources", 2015, unpublished, [Online], Available: <http://arxiv.org/ftp/arxiv/papers/1506/1506.08539.pdf>.